BIOCHEMISTRY
including biophysical chemistry & molecular biology

Article

pubs.acs.org/biochemistry

BIN1 Membrane Curvature Sensing and Generation Show Autoinhibition Regulated by Downstream Ligands and PI(4,5)P_2

Tingting Wu and Tobias Baumgart*

Department of Chemistry, School of Arts & Sciences, University of Pennsylvania, Philadelphia, Pennsylvania 19104, United States

Supporting Information

ABSTRACT: In striated muscles, invaginations from the plasma membrane, termed transverse tubules (T-tubule), function in the excitation−contraction coupling machinery. BIN1 (isoform8) plays a critical role in the biogenesis of T-tubules. BIN1 contains an N-terminal BAR domain to sense and induce membrane curvature, an isoform8-specific polybasic motif (exon10) as the phosphoinositide binding module and a C-terminal Src homology 3 (SH3) domain for the recruitment of downstream proteins such as dynamin 2. Previous studies of N-BAR domains focused on elucidating mechanisms of membrane curvature sensing and generation (MC-S&G). Less is known about how MC-S&G is regulated. We found that the SH3 domain binds to the exon10 motif more strongly compared to the proline-rich domain (PRD) of dynamin 2. Furthermore, we found that the MC-S&G ability of full-length BIN1 is inhibited on membranes lacking PI(4,5)P_2. Addition of PI(4,5)P_2 in the membrane activates BIN1 to sense and induce membrane curvature. Co-presence of the SH3 domain and exon10 motif leads to the strongest phosphoinositide-mediated control of BIN1 function. Addition of SH3 domain ligand (such as PRD peptides), as well as addition of the water-soluble PI(4,5)P_2 analogue, can both enhance the MC-S&G ability of BIN1 on membranes without PI(4,5)P_2, indicating that the key to activate BIN1 is to disrupt the exon10−SH3 interaction. The nonsense mutation K436X, found in centronuclear myopathy (CNM) patients, abolishes SH3 domain binding with either exon10 or the PRD motif, resulting in increased membrane deformation capacity. Our results suggest an autoinhibition model for BIN1 that involves a synergistic regulation by membrane composition and protein−protein interactions.

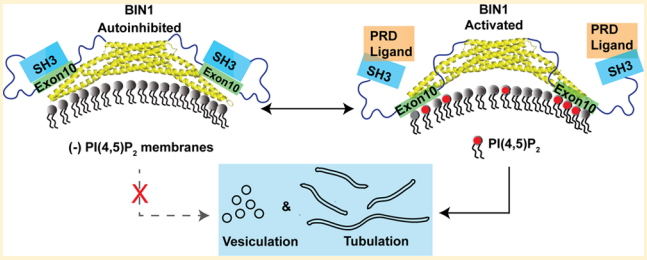

Cell membrane remodeling is accomplished through the precise temporal and spatial assembly of membrane-interacting peripheral proteins.[1,2] BIN1, also known as amphiphysin2, is such a protein involved in regulating membrane shape transitions during endocytosis and membrane trafficking.[3,4] Recently, BIN1 has drawn a lot of attention due to its implication in several human diseases.[5] BIN1 proteins are involved in cancer progression, heart failure, and late-onset Alzheimer's disease.[5,6] However, the tissue-specific pathological mechanisms and disease pathways remain unclear. BIN1's capacity for membrane deformation is contributed by its N-terminal BAR domain (Figure 1), which forms a dimerized helical bundle and binds to membranes with its positively charged concave interface.[7] BIN1 is subject to alternative splicing, leading to isoforms with specific functions in various tissues.[8,9] The BIN1 isoform8, which is enriched in striated muscle tissues, contains a polybasic sequence (exon10 motif) acting as a phosphoinositol-binding motif (Figure 1).[10,11] Past studies have shown that the isoform8 has phosphoinositide binding specificity toward PI(4,5)P_2 *in vitro*.[10] The physiological function of BIN1 isoform8 is to induce plasma membrane invaginations to form transverse tubules (T-tubules), which propagate action potentials.[3,10,12,13] In addition to the N-terminal membrane-modulating domain, the C-terminal SH3 domain serves as an adaptor for downstream ligand recruitment. SH3 domains are found in a great variety of

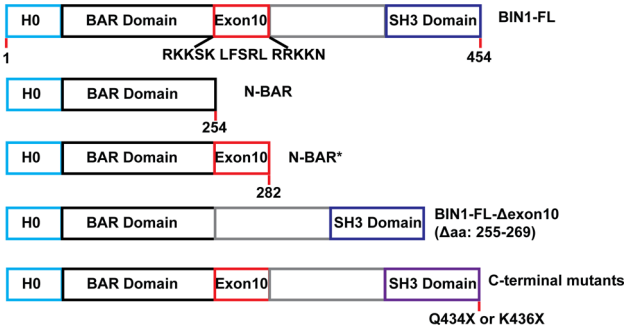

Figure 1. Domain diagrams of human BIN1 isoform8 variants investigated in this study.

BAR domain proteins.[11] SH3 domains recruit downstream proteins primarily through interaction with canonical PxxP sequences.[11,14] For instance, endophilin recruits dynamin to the neck of a clathrin-coated pit to accomplish membrane scission.[15,16] This is achieved by the hydrophobic interaction between the aromatic residues in the SH3 domain and the PxxP sequence in dynamin.[17−19]

Received: August 27, 2014
Revised: October 21, 2014
Published: October 28, 2014

Recent studies have pointed out that the SH3 domain can act not only as a recruiting module but also can regulate protein conformation and function through an autoinhibition mechanism in which the SH3 domain intramolecularly binds to the rest of the protein resulting in a closed, inactive conformation. The Haucke group provided structural evidence supporting an SH3 domain-mediated autoinhibition in syndapin1 in which the SH3 domain interacts with the BAR domain and locks syndapin into a state with compromised membrane deformation capacity.[20] Addition of dynamin1-derived PRD peptide dissociates the SH3 domain of syndapin1 from the BAR domain and rescues membrane curvature generation.[20] Such a regulatory role of SH3 domain also exists in N-BAR domain proteins. The SH3 domain of endophilin is able to complex with the N-terminal membrane-inserting helix (H_0) to regulate BAR domain dimerization kinetics.[21] Both experiments and simulations have demonstrated that H_0 is bound with the SH3 domain of the second monomer within the same dimer in solution, and this interaction slows the subunit exchange between N-BAR dimers.[21,22] Moreover, McMahon et al. reported that both endophilin and amphiphysin are autoinhibited through their SH3 domain, which impairs their membrane recruitment.[16] In the BIN1 isoform8, the binding between exon10 and SH3 domains suggests a potential mechanism for autoinhibition. Both a pull-down assay and NMR have shown that the exon10 motif can directly bind to the SH3 domain.[11] The binding interface of the SH3 domain for exon10 overlaps with that for PRD peptides.[11] Such intramolecular complexation inhibits dynamin recruitment. However, little is known about the impact of autoinhibition on the membrane remodeling capacity of BIN1, particularly in the context of MC-S&G.

We found that exon10 binds with SH3 domains with higher affinity compared to PRD due to an enrichment of basic residues in exon10. Using micropipette-assisted tether-pulling, we found that full-length BIN1 cannot sense curvature of membrane tubules lacking PI(4,5)P_2, as opposed to BIN1 variants lacking either exon10 or SH3 domain. Addition of PI(4,5)P_2 or dynamin 2-derived proline-rich domain significantly enhances the curvature sensing ability. Corresponding findings were obtained from a membrane deformation assay. We expanded our study to disease mutations in the SH3 domain and found that an SH3 truncation mutant showed loss of PI(4,5)P_2-regulated MC-S&G. Taken together, our data suggest an autoinhibition mechanism in BIN1 and synergistic activation by PI(4,5)P_2 and downstream proteins.

MATERIALS AND METHODS

Cholesterol, as well as the phospholipids 1,2-dioleoyl-*sn*-glycero-3-phosphocholine (DOPC), 1,2-dioleoyl-*sn*-glycero-3-phospho-L-serine (DOPS), 1,2-dioleoyl-*sn*-glycero-3-phosphoethanolamine (DOPE), L-α-phosphatidylinositol-4,5-bisphosphate (Brain), distearoylphosphatidylethanolamine-*N*-(biotinyl-(polyethylene glycol)2000) (DSPE-Bio-PEG2000), were purchased from Avanti Polar Lipids (Alabaster, AL). The fluorophores Alexa Fluor 488 C5-maleimide and TexasRed-1, 2-dihexadecanoyl-*sn*-glycero-3-phos-phoethanolamine triethylammonium salt (TR-DHPE) were from Invitrogen Life Technologies (Grand Island, NY). Streptavidin-conjugated microspheres with a diameter of 6 μm were from Polysciences (Warrington, PA).

DNA Construct Expression Protein Purification. DNA sequences coding for BIN1 N-BAR* (1−282) and BIN1-FL (1−454) were amplified by PCR and inserted into mKate-N1 and pGEX-4T-2 vector. The CNM-related mutation K436X and the exon10-deleted mutant were constructed by standard primer-directed PCR mutagenesis. All constructs were sequenced. BIN1 variants were expressed as GST-fusion proteins in BL21-Codon Plus (DE3)-RIL bacteria (Stratagene). Transformed cells were grown at 37 °C to reach an OD600 of 0.8, after which protein expression was induced with 1 mM IPTG for 16 h at 18 °C. Bacteria were spun down, resuspended in lysis buffer (25 mM Tris-HCl, 300 mM NaCl, 1 mM DTT, 1 mM PMSF, pH 7.4), and finally lysed on ice by tip sonication. After centrifugation, the supernatant was loaded onto a GST-affinity column equilibrated with lysis buffer. Elution was carried out using the following buffer: 50 mM Tris-HCl, 20 mM reduced glutathione, 150 mM NaCl, pH 8.0. GST-tag cleavage was accomplished through thrombin digestion at room temperature for 4 h, and BIN1 was further purified by ion exchange and gel filtration (GE Healthcare). BIN1 was labeled on its endogenous cysteine residues, through overnight incubation with Alexa 488 C5-maleimide (Invitrogen) at 4 °C. Passing three times through a desalting column removed free fluorophores. Protein concentrations were measured by standard Bradford assay (Thermo Scientific, 0.5%−1% uncertainty in protein concentration, n = 3), and concentrations of fluorophores were determined by absorbance at 494 nm (assuming a molar extinction coefficient of 71 000 cm^{-1} M^{-1}). The labeling efficiency was calculated as follows: Labeling efficiency [%] = Alexa 488 concentration/protein concentration × 100. All protein samples used in our study were ultracentrifuged after thawing to remove potential aggregates. Before each experiment, protein concentrations were assessed via Bradford assay. No sample stored at 4 °C for longer than 1 week was used in this study.

Peptide Synthesis and Purification. The exon10 peptide (sequence: RKKSKLFSRLRRKKN) and dynamin 2-derived proline-rich domain peptide (sequence: PPQIPSRPVRIPPGI) were synthesized via solid phase peptide synthesis, using 9-fluorenylmethoxycarbonyl (FMOC) chemistry. After resin cleavage, peptides were purified by reverse-phase high-performance liquid chromatography (HPLC). The purity of the synthesized peptides was >95%. The molecular weight of the peptide was confirmed by mass spectrometry. The rhodamine-conjugated PRD peptides were labeled at the N-terminus.

Cell Culture, Transfection, and Confocal Fluorescence Imaging. Myoblasts (C2C12 cells) were cultured in DMEM medium containing 10% fetal bovine serum (FBS) (Invitrogen). Cells were grown in MatTek glass bottom culture dishes to 95% confluency before transfection. Transfection was done via Lipofectamin2000 (Life Technologies, Invitrogen), using 1.5 μg of mKate-tagged DNA and incubation at 37 °C, 5% CO_2 for 5 h before change to culture medium. After 24 h, cells were imaged with a confocal microscopy (FV300) laser scanning system based on an inverted microscope IX81 (Olympus, Center Valley, PA) using a 60×, 1.2 NA water immersion lens (Olympus). Images were imported into, and processed with, ImageJ.

Liposome Preparation. Liposomes used in the tubulation assay were prepared using a composition of 64% DOPC/26% DOPS/10% DOPE, or 68% DOPC/20% DOPS/2% PI(4,5)-P_2/10% DOPE. Mixtures of lipids were air-dried to form thin films and left under a vacuum for at least 2 h before rehydration in 20 mM Hepes, 150 mM NaCl, pH 7.4 buffer. The final lipid concentration was 1 mg/mL. After sonication for 15 min,

liposomes were extruded through 400 nm nuclepore membranes (Whatman) five times. All liposome dispersions were stored at 4 °C.

GUVs (64% DOPC/26% DOPS/10% DOPE or 68% DOPC/20% DOPS/2% PI(4,5)P_2/10% DOPE) were prepared by the standard method of electroswelling in 0.3 M sucrose solution.[23] 0.5% DSPE-Bio-PEG2000 and TR-DHPE were also included in the lipid mixtures. The osmolarity of GUV dispersions was measured with a micro-osmometer (Advanced Instruments Inc., Norwood, MA).

Liposome Tubulation Assay. BIN1 variants were incubated with liposomes (lipid composition described above) in 20 mM Hepes, 150 mM NaCl, pH 7.4 buffer at room temperature for 30 min. The final protein concentration was 5 μM, and the lipid concentration was 0.2 mg/mL. Then samples were adsorbed to carbon/Formvar supported copper grids (Electron Microscopy Science, Hatfield, PA) for 5 min. Grids were washed with buffer and blotted on a filter paper (Whatman) to remove excess sample. The grids were stained with 2% (w/v) uranyl acetate for 1 min. Excess stain was washed away, and the samples were dried at room temperature. Samples were observed with a JEM 1011 transmission electron microscope (JEOL, USA) with an accelerating voltage of 100 kV. Images were analyzed with ImageJ.

BIN1 Curvature Sorting Measurements. Protein curvature sorting measurements were carried out in a chamber constructed from glass slides, containing GUV dispersions and protein solution. Two micropipettes (World Precision Instruments, Sarasota, FL), which were fabricated with the help of a pipette puller and a microforge, were inserted into the sample chamber through a three-dimensional motorized manipulator system (Luigs and Neumann, Ratingen, Germany). The lateral tension of micropipette-aspirated vesicles was controlled by adjusting the height of a connected water reservoir, and measured by a pressure transducer with a DP-28 diaphragm (Validyne Engineering, Los Angeles, CA). Membrane tethers were pulled with the help of a streptavidin-coated bead that was moved with a second aspiration pipette. Kalman-averaged images of the tether cross section (*xz* plane, which was orthogonal to the axis of the tether) allowed measurement of the tether fluorescence intensities. These images were obtained using a stepwidth of 0.15 μm and a total imaging depth of 6 μm, and were background-corrected and analyzed in an elliptical region of interest to obtain the protein and lipid intensity signals under varying tensions. For each protein, at least five independent experiments were carried out and binned after analysis.

Isothermal Titration Calorimetry (ITC) Measurements. ITC binding reactions were performed with a MicroCal iTC200 system (GE Healthcare, Life Sciences) at 25 °C. Protein and peptide samples were dialyzed side by side in 20 mM Hepes, pH 7.4 buffer containing 0 mM, 50 mM, or 150 mM NaCl. A total of 40 μL of the ligand in the injection syringe was titrated into a 200 μL reaction cell in 16 or 20 cycles. The duration of each injection was 4 or 5 s with an interval of 120 s between injections. ITC data from at least four independent experiments were analyzed with MicroCal's custom scripts in Origin 7.0 (OriginLab). Integrated heats from all the binding reactions could be fitted well with a single-site binding model. Concentrations used in the ITC measurement were as follows. Exon10-SH3 domain binding: 500 μM exon10 peptide in the injection syringe and 50 μM GST-SH3 domain in the reaction cell; PRD-SH3 domain binding: 1 mM PRD peptide in the injection syringe and 50 μM GST-SH3 domain in the reaction cell; exon10-SH3/K436X mutant binding: 500 μM exon10 peptide in the injection syringe and 50 μM GST-SH3/K436X mutant in the reaction cell; exon10−IP3 binding: 500 μM exon10 peptide in the injection syringe and 25 μM IP3 in the reaction cell.

RESULTS

Exon10 Motif Binds to the SH3 Domain More Strongly than the PRD Peptide. We compared the exon10−SH3 domain to the PRD−SH3 domain binding affinity through ITC. We first titrated the synthetic exon10 peptides (RKKSKLFSRLRRKKN) into recombinant GST-SH3 domains (derived from BIN1) (Figure 2A,B). Because of the basic nature of the exon10 peptide, we investigated the effects of the salt concentration on exon10-SH3 domain binding. Consistent with expectation, lowering ionic strength increases the affinity of the exon10 peptide for the SH3 domain, indicating that the exon10−SH3 binding is driven by electrostatic interactions (Figure 2C). Fitting with a single site binding model yielded a dissociation constant K_d of 3.9 ± 0.2 μM in 50 mM NaCl buffer (Figure 2A, data are represented as mean ± standard error of the mean (SEM) of at least six trials) and 11.3 ± 0.6 μM in 150 mM NaCl buffer (Figure 2B). Of course, this affinity of SH3−exon10 interactions will be enhanced in the full-length protein through the tethering effect because the binding partners are localized within the same polypeptide chain.[24,25] When the exon10 peptide was titrated into BIN1-FL protein, the reaction did not reach saturation rendering the determination of K_d and stoichiometry inaccurate due to the low affinity for the full-length protein (data not shown). The reduced affinity of exon10 binding to full-length protein compared to SH3 domain is consistent with a competition of free exon10 with the endogenous exon10−SH3 complex and thus supports an autoinhibition model involving exon10−SH3 binding.

SH3 domains are known proline-rich domain recruiters.[26] To evaluate this binding strength, we titrated a PRD peptide (PPQIPSRPVRIPPGI, derived from dynamin 2) into a GST−SH3 domain solution. As for exon10−SH3 domain binding, ionic strength-sensitive PRD−SH3 domain binding was observed, albeit with lower binding affinity (Figure 2A,B). The K_d obtained for the SH3−PRD interaction was 13.7 ± 1.2 μM and 68.3 ± 4.9 μM in 50 mM and 150 mM NaCl buffer, respectively (Figure 2A,B). The salt effect on the dissociation constant agrees with the extensive patch of negative electrostatic potential covering a large portion of the dynamin binding site of the SH3 domain[14] and two conserved Arg residues in the PxRPxR consensus sequence[26] of the dynamin 2 PRD domain. The weaker binding affinity of the PRD peptide to the SH3 domain compared to the exon10 motif (Figure 2C) further supports the notion that the SH3 domain can be masked from its PRD ligand due to the stronger exon10−SH3 interaction. Ligand recruitment may require sufficiently high concentration of the downstream proteins to compete with the exon10 motif. Alternatively, other regulatory mechanisms may release the SH3 domain, for example, through phosphoinositide binding during plasma membrane binding.[11]

It is currently unclear how exactly the exon10 motif interacts with membranes. CD spectra of exon10 peptides in solution, as well as on (+) PI(4,5)P_2 membranes, reveal a characteristic peak of random coils at 204 nm (Figure S1, Supporting Information).[27] This observation implies that exon10 peptides,

dx.doi.org/10.1021/bi501082r | *Biochemistry* 2014, 53, 7297−7309

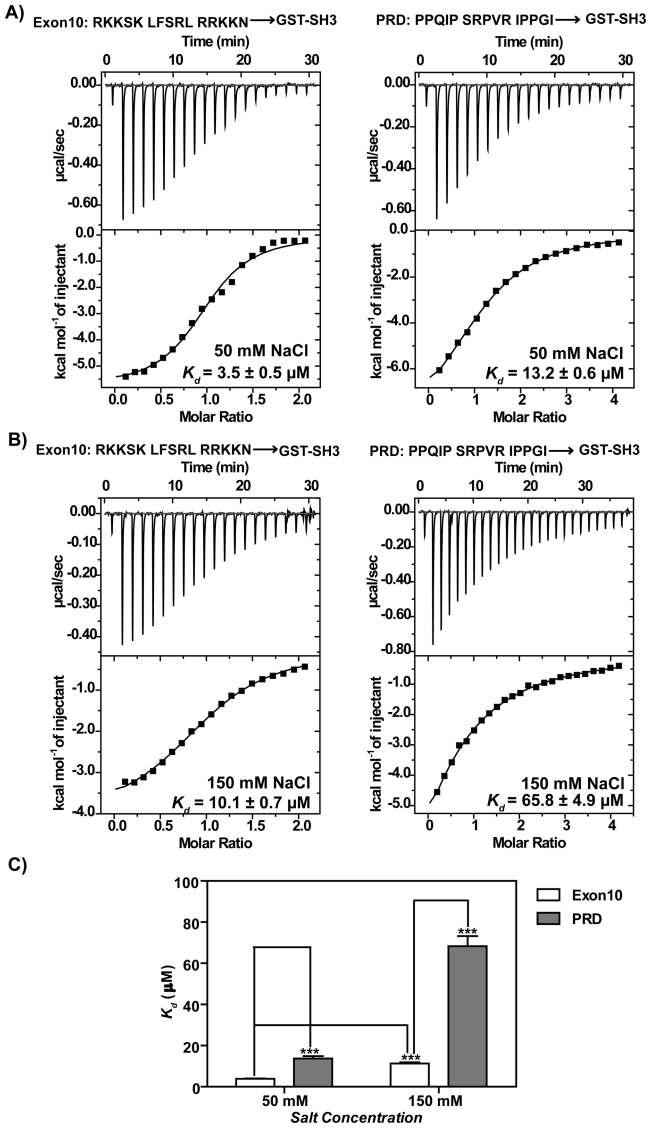

Figure 2. The binding affinity of the exon10−SH3 complex is higher than that of SH3−PRD. Both are dependent on solution ionic strength. The association between exon10−SH3 and PRD−SH3 was characterized by ITC in which 500 μM exon10 peptide or 1 mM PRD (derived from dynamin 2) was titrated into 50 μM GST-SH3 domain (derived from BIN1) in (A) 20 mM Hepes, 50 mM NaCl, pH 7.4 buffer and (B) 20 mM Hepes, 150 mM NaCl, pH 7.4 buffer. Curves were fitted by a single-site binding model, and the dissociation constant, K_d, and the fit standard error are shown for each titration. Of note, the stoichiometry, N, of each titration is found to be close to 1, indicating a single SH3 domain binding site for both ligands. Reducing the salt concentration enhances both exon10−SH3 and PRD−SH3 association. (C) Comparison of averaged dissociation constants at varied solution conditions. Exon10 binds to SH3 domain stronger than the PRD peptides. Student t-test was performed to assess the statistical significance. ***$p < 0.005$.

unlike the membrane-inserting, amphipathic helices in N-BAR domain proteins,[28−31] do not adopt secondary structure upon membrane association. It is likely that the exon10 motif may not be able to penetrate into the hydrophobic core of the lipid bilayer to induce membrane curvature.[32] This finding is compatible with the highly charged nature of the exon10 sequence. Furthermore, corresponding behavior has been found for the effector domain of the myristoylated alanine-rich C-kinase substrate (MARCKS-ED) peptide, which is another membrane binding peptide enriched in basic residues.[33,34]

Curvature Sensing Ability of BIN1-FL Is Inhibited on PI(4,5)P_2-Absent Membranes. It has been shown that N-BAR domains function as curvature sensors.[35−37] The curvature sensing process is defined as enrichment of proteins on curved membranes, and in turn, stabilization of tubular membranes. This is crucial to a great number of cellular processes. Particularly, BIN1 is responsible for the membrane tubulation process in myocytes. We have previously demonstrated that the N-BAR domain from BIN1 preferentially partitions onto cylindrical tethers compared to flat membranes.[37] We next asked how the exon10−SH3 domain interaction affects MC-S&G and whether phosphoinositides regulate the BIN1−membrane interaction through a mechanism similar to their regulation of dynamin recruitment.[11] To compare membrane curvature sensing of BIN1-FL on membranes with and without PI(4,5)P_2, we used a micropipette-assisted tether-pulling assay.

For this purpose, the following two lipid compositions were chosen that are meant to mimic inner leaflet headgroup compositions (but to prevent lipid demixing): (1) 68% DOPC/20% DOPS/10% DOPE/2% PI(4,5)P_2 (abbreviated as (+) PI(4,5)P_2); (2) 64% DOPC/26% DOPS/10% DOPE (abbreviated as (−) PI(4,5)P_2). The charge densities in these two compositions are similar assuming that the charge of PI(4,5)P_2 is −3 at physiological buffer conditions.[38−41] A tubular membrane was pulled from a pipette-aspirated giant unilamellar vesicle (GUV) by a polystyrene bead, and membrane tension was controlled by the aspiration pressure in the micropipette. The radius of the cylindrical tubule is inversely related to membrane tension. The membrane curvature of the tether can therefore be well controlled by changing the aspiration pressure. Figure 3A,B shows fluorescence intensities of the tether cross-section in both protein and lipid channel plotted against membrane tension. On (+) PI(4,5)P_2 membranes, by increasing membrane tension, the protein fluorescence signals on the tether cross sections were observed to increase, while the fluorescence intensities for the lipid channel were decreasing (Figure 3A). In sharp contrast, for (−) PI(4,5)P_2 membranes, both protein and lipid fluorophore fluorescence intensities decreased when the tether radius decreased (Figure 3B). To obtain a quantitative characterization of the curvature sensing ability of BIN1-FL, we calculated the ratio I_r of protein (green label) and lipid (red label) fluorescence intensities on the tether ($I_r = I^t_{green}/I^t_{red}$) and divided it by the corresponding ratio on the vesicle ($I^0_r = I^v_{green}/I^v_{red}$). This partitioning ratio, I_r/I^0_r, can be shown to be proportional to the protein density on the tether normalized by the protein density on the GUV.[42,43] I_r/I^0_r has been observed for several (albeit not all) proteins to vary linearly with the square root of membrane tension $\Sigma^{1/2}$, in accordance with a first-order thermodynamic theory.[42−44] The slope of the $I_r/I^0_r - \Sigma^{1/2}$ relationship is related to the curvature sorting ability of a given protein. We found significant curvature sorting of BIN1-FL on membranes containing PI(4,5)P_2. However, on (−) PI(4,5)P_2 membranes, the partitioning ratio barely increases with the square root of membrane tension yielding a linear fit slope substantially smaller compared to the case of (+) PI(4,5)P_2 membranes (Figure 3C).

We note that in the curvature sensing assay, we selected for analysis GUVs displaying comparable protein fluorescence intensities, in order to exclude the influence of protein density on curvature coupling.[36] We found that BIN1-FL binds to (±)

dx.doi.org/10.1021/bi501082r | Biochemistry 2014, 53, 7297−7309

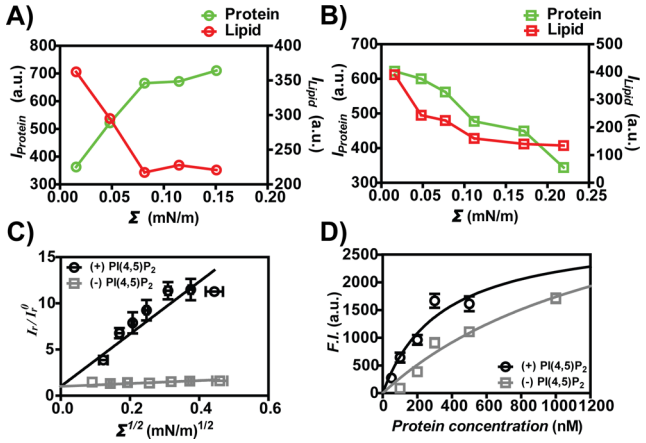

Figure 3. Curvature sensing ability of BIN1-FL is inhibited on membranes lacking PI(4,5)P_2. Alexa488 conjugated BIN1-FL (40 nM) was incubated with TexasRed-DHPE labeled GUVs. A GUV was aspirated by a micropipette, and membrane tension was controlled by the aspiration pressure. A tether was pulled by an aspirated streptavidin-coated polystyrene bead, and the confocal images of the tether cross sections were recorded. Fluorescence intensities of protein and lipid in tether cross sections were plotted against membrane tension Σ. The protein intensities responded differently to changes in the membrane tension on (A) (+) PI(4,5)P_2 membranes and (B) (−) PI(4,5)P_2 membranes. (C) Data from 10 vesicles were binned (vertical error bars represent SEM; horizontal error bars show SEM of the square root of membrane tension) for two different lipid compositions. The solid lines show linear fits to guide the eye. Membrane curvature-coupled protein partitioning behavior is only observed on (+) PI(4,5)P_2 membranes. (D) demonstrates similar protein adsorption isotherm on (+) PI(4,5)P_2 or (−) PI(4,5)P_2 GUVs. Error bars: SEM. Lipid compositions: (+) PI(4,5)P_2: 68% DOPC/20% DOPS/10% DOPE/2% PI(4,5)P_2; (−) PI(4,5)P_2: 64% DOPC/26% DOPS/10% DOPE. Buffer: 50 mM NaCl, Hepes buffer, pH 7.4. F.I.: fluorescence intensity; a.u.: arbitrary unit.

PI(4,5)P_2 GUVs with comparable affinities. Figure 3D shows a titration of BIN1-FL into (±) PI(4,5)P_2 GUVs. The dissociation constant K_d was obtained by fitting a Langmuir isotherm model to the titration curve. BIN1-FL binds to (+) PI(4,5)P_2 membranes with a K_d of 371 ± 59 nM and to (−) PI(4,5)P_2 membranes with a K_d of 883 ± 165 nM, respectively. We only fitted data for which membrane tubulation was not visible on GUVs. The membrane binding affinity was slightly increased on the PI(4,5)P_2-present membrane possibly due to the multivalency of the PI(4,5)P_2 headgroup[39] and/or increased membrane penetration driven by PI(4,5)P_2.[45] The effect of PI(4,5)P_2 on the curvature sensing ability of BIN1-FL is more dramatic than the effect on membrane binding. Overall, our data suggest that BIN1 senses membrane curvature in a PI(4,5)P_2-dependent manner.

The PI(4,5)P_2-Dependent Curvature Sorting Ability Requires Co-Presence of SH3 Domain and exon10 Motif. We next aimed to evaluate possible mechanisms responsible for the differing curvature sorting abilities of BIN1 on (±) PI(4,5)P_2 membranes. Specifically, we asked whether exon10−SH3 association contributes to the dependency of BIN1 function on lipid composition. Therefore, curvature sorting was determined on (±) PI(4,5)P_2 compositions for truncated BIN1 versions (Figure 1) meant to disrupt SH3−exon10 interactions: BIN1 N-BAR (aa: 1−254, Figure 4A), BIN1 N-BAR* (aa: 1−282, Figure 4B), and BIN1-FL-Δexon10 (BIN1-FL-Δaa: 255−269, Figure 4C). The PI(4,5)-

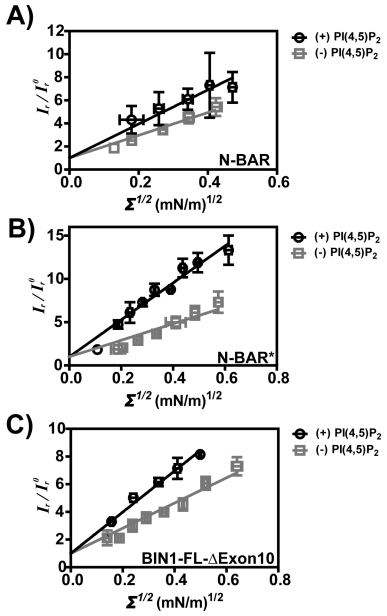

Figure 4. Curvature sensing ability of BIN1 variants lacking either exon10 or SH3 domain is less dependent on PI(4,5)P_2 than BIN1-FL. Normalized ratio of fluorescence intensities between protein and lipid channels were plotted against the square root of membrane tension for (A) N-BAR (400 nM), (B) N-BAR* (40 nM), and (C) BIN1-FL-Δexon10 (400 nM) on GUVs (±) PI(4,5)P_2. Error bar: SEM.

P_2-dependent curvature sorting was weaker in mutants lacking SH3 domain and/or exon10 (Figure 4A−C). These observations demonstrate that the co-presence of the exon10 and SH3 domain is responsible for hindering curvature coupling of BIN1 on membranes without PI(4,5)P_2. We acknowledge that the curvature sensing ability of BIN1 truncates is higher on (+) PI(4,5)P_2 compared to (−) PI(4,5)P_2 membranes, which may indicate specific effects of PI(4,5)P_2 on membrane interactions with BAR domains.[45] However, all truncation variants do show significant curvature sorting behavior on (−) PI(4,5)P_2 membranes (Figure 4A−C), different from the full-length protein (Figure 3C). Thus, only for BIN1-FL, membranes lacking PI(4,5)P_2 result in an inactive state incapable of sensing membrane curvature. Addition of PI(4,5)P_2 to the membrane allows exon10 to interact with the membrane and releases the SH3 domain. Deletion of either SH3 domain or exon10 motif disrupts this regulatory mechanism. Taken together, BIN1 is autoinhibited via an exon10−SH3 complex and can be activated through phosphoinositides in the membrane.

Membrane Curvature Generation Ability of BIN1-FL Is Compromised on (−) PI(4,5)P_2 Membranes. BIN1 is not only a membrane curvature sensor but also a curvature generator.[29,30] N-BAR domains from BIN1 can induce membrane tubulation.[37] To investigate if the curvature generation capacity of BIN1 is autoinhibited and regulated by phosphoinositides, we characterized the membrane morphologies modulated by BIN1 and its variants via negative staining transmission electron microscopy (TEM). In the absence of BIN1 protein, liposomes did not show membrane tubules for either (+) PI(4,5)P_2 or (−) PI(4,5)P_2 composition (Figure 5A). Upon the incubation with 5 μM BIN1-FL, tubules with a diameter of 28.4 ± 0.7 nm were generated from (+) PI(4,5)P_2 membranes. Vesiculation (individual vesicles boxed in Figure 5A) was observed as well, which is a general feature for N-BAR domain containing amphipathic membrane-inserting heli-

dx.doi.org/10.1021/bi501082r | Biochemistry 2014, 53, 7297−7309

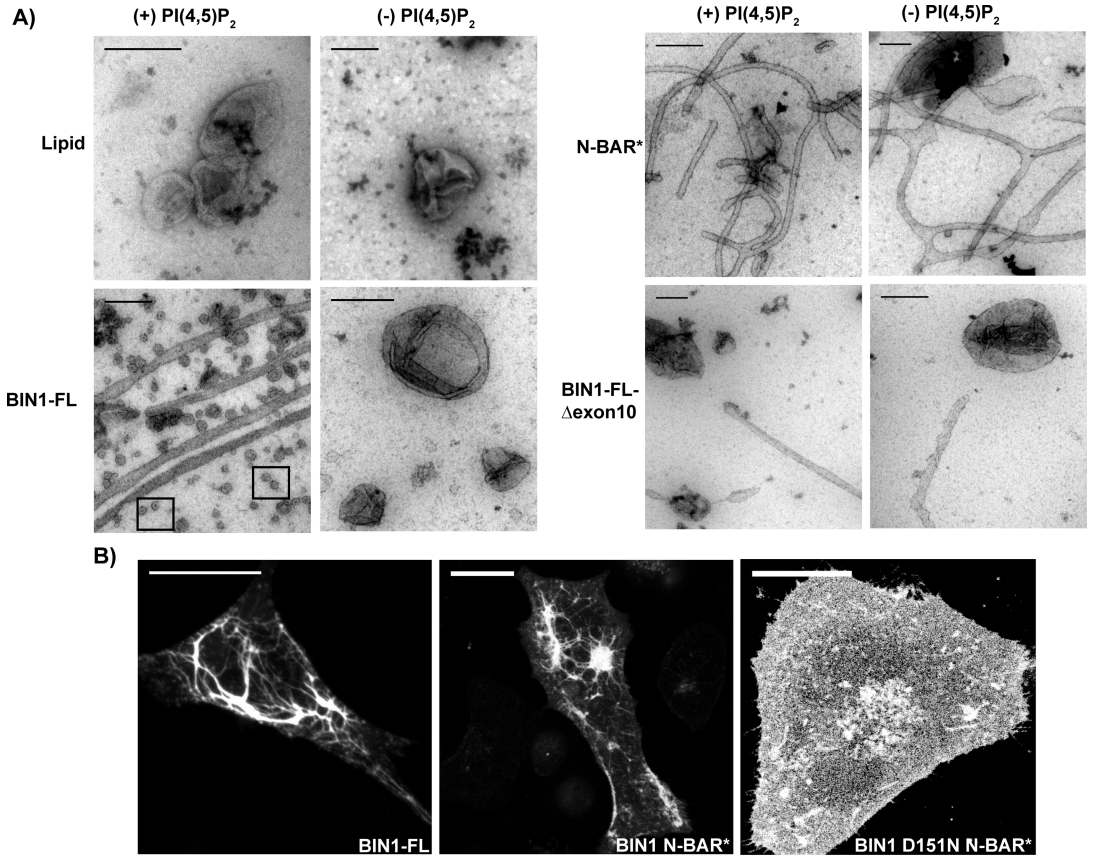

Figure 5. Tubulation capacity of BIN1-FL is autoinhibited on (−) $PI(4,5)P_2$ membranes *in vitro*. The autoinhibition in curvature generation requires co-presence of exon10 and SH3 motif. (A) Electron micrographs of LUVs (±) $PI(4,5)P_2$ (0.2 mg/mL) incubated with 5 μM BIN1-FL, N-BAR* and BIN1-FL-Δexon10 in 20 mM Hepes, 150 mM NaCl, pH 7.4 at room temperature. Samples were negatively stained and imaged by TEM. In the lipid control sample, no membrane tubules were observed. Upon the addition of BIN1-FL, tubulation and vesiculation (generation of vesicles with the diameter less than 30 nm, boxed in the BIN1-FL/(+) $PI(4,5)P_2$ panel) were induced only on the $PI(4,5)P_2$-containing membrane. Much less curvature generation through BIN1-FL was observed in membranes without $PI(4,5)P_2$. Neither N-BAR* nor BIN1-FL-Δexon10 showed lipid composition-dependent tubulation capacity. Reduced membrane reshaping ability of BIN1-FL-Δexon10 variant is due to the lower membrane binding capacity. Scale bar: 200 nm. (B) Confocal images of C2C12 myoblasts transfected with BIN1-FL, N-BAR* or N-BAR* D151N mutant conjugated with red fluorescence protein, mKate, at the C-terminus. *In vivo*, membrane tubules are induced both by BIN1-FL and N-BAR*, indicating release of autoinhibition at the plasma membrane. Scale bar: 20 μm.

ces.[30,46] However, significantly less membrane shape changes were observed on (−) $PI(4,5)P_2$ liposomes. The morphology of those vesicles was similar to the ones in the lipid control (Figure 5A). This finding confirms that the curvature generation ability of full-length protein is inhibited on (−) $PI(4,5)P_2$ membranes, in correspondence with the curvature sensing ability of BIN1-FL.

Next we aimed to investigate the hypothesis that the inhibited curvature generation results from the co-presence of SH3 domain and exon10. We therefore studied the tubulation ability of BIN1 N-BAR* and BIN1-FL-Δexon10 on the two lipid compositions (±) $PI(4,5)P_2$ (Figure 5A). As expected, BIN1 N-BAR* domains are able to induce spontaneous tubulation from both lipid compositions. For the BIN1-FL-Δexon10 mutant, reduced tubulation was observed. The number of membrane tubules decreased compared to BIN1-FL and N-BAR*. This can be explained by the compromised electrostatic interactions of BIN1-FL−Δexon10 with the membrane. The membrane deformation ability of BIN1-FL−Δexon10 is similar in the absence or presence of $PI(4,5)P_2$ in the membrane. We conclude that as for curvature sensing, the $PI(4,5)P_2$-dependent tubulation ability of BIN1-FL is caused by the co-presence of SH3 domain and exon10.

We next asked if BIN1 is autoinhibited at the plasma membrane. When transfecting plasmids encoding a red fluorescent protein conjugated to BIN1 N-BAR* or BIN1-FL in C2C12 myoblasts, membrane tubulation was caused by both constructs. As shown in Figure 5B, invaginations from the cell membrane were induced by both N-BAR* and BIN1-FL, suggesting that autoinhibition of BIN1's membrane sculpting ability is released at the plasma membrane. Contrarily, a tubulation-defective version of N-BAR* (mutation D151N within the N-BAR* domain) leads to essentially homogeneously distributed fluorescence in cells (rightmost panel in Figure 5B). This observation is in accordance with the compromising effects of disease-related mutations in BAR domains on membrane deformation and further supports the role of full-length BIN1 in T-tubule biogenesis *in vivo*.[3,10] The spontaneous activation of BIN1-FL at plasma membranes likely is due to their specific lipid composition. It is known that $PI(4,5)P_2$ is enriched in the inner leaflet of the plasma membrane.[47] Given our observations that the binding of exon10 to $PI(4,5)P_2$ in the membrane switches BIN1 into an active conformation allowing sensing and induction of membrane curvature (Figures 3 and 5), BIN1-FL likely is

dx.doi.org/10.1021/bi501082r | *Biochemistry* 2014, 53, 7297−7309

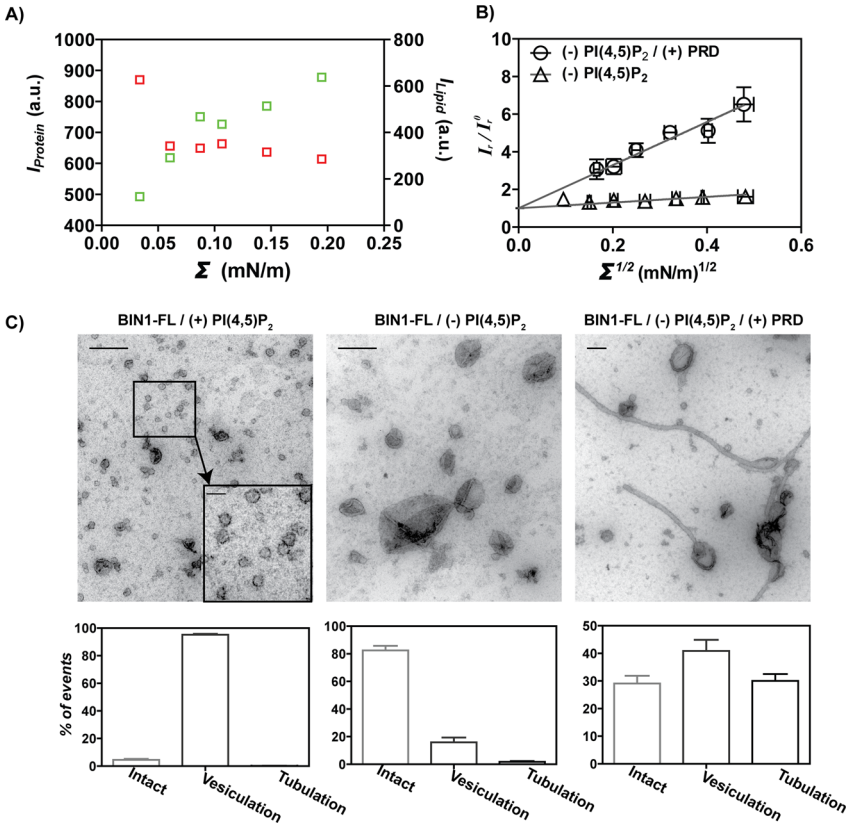

Figure 6. Addition of PRD increases the curvature sensing and generation capacity of BIN1 on (−) $PI(4,5)P_2$ membranes. (A) Membrane curvature sensing assay was performed using the (−) $PI(4,5)P_2$ lipid composition in 20 mM Hepes, 50 mM NaCl, pH 7.4 buffer. 40 nM BIN1-FL was preincubated with 200 μM dynamin 2-derived PRD peptide for 15 min prior to the experiment. A membrane tether was formed as described in the Materials and Methods. Fluorescence intensities of protein and lipid on the tether cross sections were measured and plotted against membrane tension Σ. BIN1-FL enriched on the tether when increasing membrane tension as opposed to Figure 3B where PRD was absent. Panel (B) demonstrates that association with PRD peptide activates the curvature sensing ability of BIN1-FL on (−) $PI(4,5)P_2$ membranes. (C) Electron micrographs of 5 μM BIN1-FL or 5 μM BIN1-FL mixed with 200 μM PRD peptide interacting with LUVs (±) $PI(4,5)P_2$ in the 20 mM Hepes, 50 mM NaCl buffer. Samples were stained with 2% (w/v) uranyl acetate solution for contrast enhancement. Scale bar: 200 nm. Morphologies of the liposomes were categorized into three types: intact vesicles: vesicles with diameters larger than 30 nm; vesiculation: vesicles with diameter less than 30 nm; and tubulation. BIN1-FL induces vesiculation of (+) $PI(4,5)P_2$ membranes but not of (−) $PI(4,5)P_2$ liposomes. The inset shows an enlarged image of the vesicles in the boxed area. The scale bar in the inset is 50 nm. Addition of PRD peptide results in both increased tubulation and vesiculation from the (−) $PI(4,5)P_2$ LUVs. The percentage of the three membrane morphologies was quantified through image analysis.

activated upon plasma membrane binding and remains inactive in the cytosol or other intracellular compartments.

We hypothesize that another way to activate BIN1 is through dissociation of the exon10−SH3 complex by SH3 domain association with a ligand, such as dynamin 2 or other PRD domain containing proteins. Such an activation mechanism has been proposed in the autoinhibition model of syndapin, in which the addition of the PRD peptide rescued the tubulation ability of syndapin.[20,46] Consistent with this finding, ligand binding to the SH3 domain of the cytoskeletal protein IRSp53 leads to activation of this protein.[24] We therefore next tested if downstream ligand recruitment affects BIN1 autoinhibition.

PRD Peptide Releases Autoinhibition of BIN1-FL Curvature Sensing and Generation. So far, we have demonstrated that $PI(4,5)P_2$ in the membrane modulates membrane curvature sensing and generation ability of BIN1. In order to test our hypothesis that SH3 domain ligands are able to release autoinhibition, we preincubated BIN1-FL with 200 μM PRD (well above K_d at the ionic strength chosen; see Figure 2) peptide prior to performing curvature sensing measurements on (−) $PI(4,5)P_2$ membranes. Co-incubation with PRD peptide enhanced the protein partitioning onto the membrane tether. The protein fluorescence intensities increased while the membrane tether got narrower as indicated by the drop in lipid fluorophore intensities (Figure 6A). Note that the trend of protein signal changing with membrane tension (green data points in Figure 6A) is opposite compared to the one in Figure 3B, although no $PI(4,5)P_2$ was present in the membrane. The slope of the $I_r/I_r^0-\Sigma^{1/2}$ relationship deviates significantly from the case in which the PRD was absent (Figure 6B). The activation of BIN1-FL through PRD peptides on (−) $PI(4,5)P_2$ membranes further supports our hypothesis that the exon10−SH3 complexation compromises the membrane remodeling function of BIN1. Either the binding to $PI(4,5)P_2$ (by exon10) or PRD motif (by SH3 domain) can release the autoinhibitory interaction and induce BIN1 to adopt a conformation suitable for membrane remodeling.

We next investigated if coincubation with PRD peptide is able to rescue the membrane deformation ability as well. PRD peptide (200 μM) was first incubated with BIN1-FL (5 μM) before addition to (−) $PI(4,5)P_2$ LUVs. As a control, BIN1-FL was added (at the same concentration) to (±) $PI(4,5)P_2$ LUVs without PRD peptides. The tubulation assay was performed in 50 mM NaCl instead of 150 mM (Figure 5) due to the

dx.doi.org/10.1021/bi501082r | Biochemistry 2014, 53, 7297−7309

dependence of PRD-SH3 binding on salt concentration and to achieve consistency with experimental conditions used for the tether-pulling assay. TEM images of each condition are shown in Figure 6C. In order to quantitatively evaluate the membrane curvature generation capacity, we divided the observed morphologies into three groups: (1) vesiculation: liposomes with diameters less than 30 nm; (2) tubulation: elongated membranes; and (3) unchanged vesicles with diameters larger than 30 nm. We consider both small vesicles and tubules as products of membrane curvature generation.[30] Consistent with Figure 5, BIN1-FL produces membrane curvature only on (+) $PI(4,5)P_2$ membranes. Curvature induction by BIN1-FL at low ionic strength predominantly leads to vesiculation. As shown in the boxed area in Figure 6C, uniformly sized vesicles were formed after incubating BIN1-FL with (+) $PI(4,5)P_2$ liposomes. However, vesiculation and tubulation are rarely seen in the (−) $PI(4,5)P_2$ sample. Preincubation of the PRD peptide with full-length protein effectively increased the number of both membrane tubules and vesiculated liposomes in the (−) $PI(4,5)P_2$ sample. To obtain a quantitative evaluation of BIN1 activation achieved by association with PRD peptides, the percentages of three morphological groups are plotted in Figure 6C. Over 90% of the membrane morphologies induced by BIN1 from the (+) $PI(4,5)P_2$ membranes belong to vesiculation, while more than 80% of the events are intact vesicles in the case of (−) $PI(4,5)P_2$ membranes. Co-incubation with PRD peptides resulted in an enhancement of tubulation and vesiculation abilities of BIN1-FL and a decrease in the occurrence of intact vesicles for membranes lacking $PI(4,5)P_2$.

To summarize, we demonstrated that adding PRD peptides activates both curvature sensing and curvature generation capacity of BIN1, in agreement with our autoinhibition model. The key to activate BIN1 membrane remodeling ability is to dissociate the exon10−SH3 mediated inhibitory complex. Our model indicates a regulation/activation mechanism in BIN1 through plasma membrane localization and protein−protein interactions.

Analogue of $PI(4,5)P_2$ Headgroup Releases the Inhibited Membrane Curvature Sensing Ability of BIN1 on (−) $PI(4,5)P_2$ Membranes. So far, we have shown that $PI(4,5)P_2$ in the membrane, or the association with an SH3 domain ligand, activates BIN1 MC-S&G. To further support this finding, we asked if addition of a water-soluble $PI(4,5)P_2$ analogue leads to release of BIN1 autoinhibition on (−) $PI(4,5)P_2$ membranes. We chose D-myo-inositol-1,4,5-triphosphate (IP3) as an analogue of the $PI(4,5)P_2$ headgroup. We used ITC to find out if IP3 is able to bind to the exon10 motif and to determine the corresponding affinity. The binding between exon10 peptide and IP3 is dependent on ionic strength. The averaged K_d of exon10 binding with IP3 in 0 mM NaCl buffer is 1.02 ± 0.1 μM, while the K_d in 50 mM NaCl buffer is 5.6 ± 0.8 μM (Figure 7A). At physiological ionic strength, the K_d was too high to be obtainable by ITC, implying that the interaction between exon10 peptides and IP3 molecules is dominated by electrostatic interactions. Since the salt concentration used for the curvature sensing assay was 50 mM, we chose to carry out curvature sensing measurements in the presence of 20 μM IP3 (around four times higher than K_d at this ionic strength) and 40 nM BIN1-FL incubated with (−) $PI(4,5)P_2$ membranes. If IP3 were able to dissociate exon10 from the SH3 domain, then a release in autoinhibition would be expected. Indeed, we observed an enhancement of protein localization on the membrane tether. The partitioning ratio I_r/I_r^0 is observed to always be higher compared to BIN1-FL alone on (−) $PI(4,5)P_2$ membranes (Figure 7B). However, the released curvature sensing ability (as indicated by the slope in Figure 7B) is weaker in the presence of IP3 than in the case of the BIN1-FL protein alone on (+) $PI(4,5)P_2$ membranes (Figure 3C). There are two possible explanations for the partially released curvature sensing function. First, membrane binding of exon10 may be required to fully release the MC-S&G capacity of BIN1. Second, it is reasonable to assume that the binding affinity of exon10 motif with membranous $PI(4,5)P_2$ is stronger than with IP3. This is a common effect for protein−membrane interactions that are enhanced by proximity, local ionic strength, and favorable orientation achieved on the surface of membranes.[48−50]

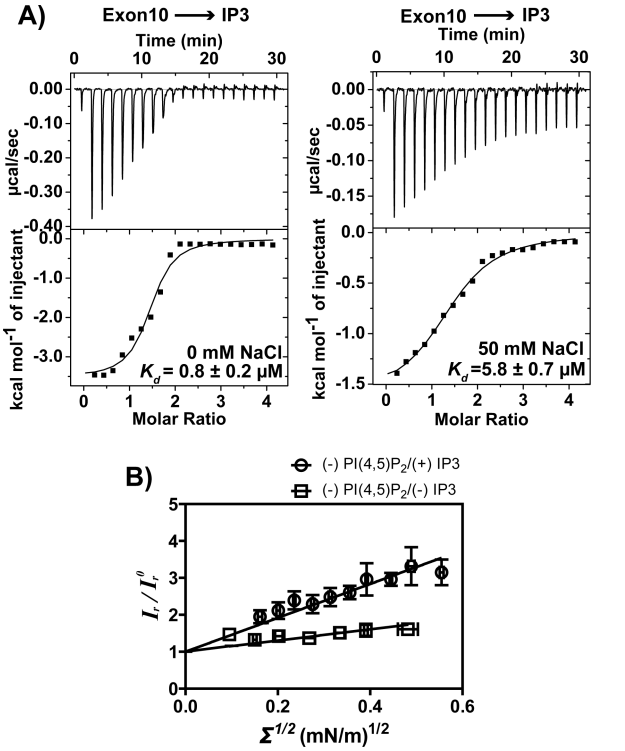

Figure 7. IP3 (water-soluble analogue of $PI(4,5)P_2$ headgroup) binds to exon10 motif and releases membrane curvature sensing ability. (A) *In vitro* binding affinity between exon10 and IP3 was characterized by the ITC measurement in which 500 μM exon10 peptides were added to 25 μM IP3 in buffer containing 0 mM or 50 mM NaCl. The interaction between exon10 peptide and IP3 was significantly affected by solution ionic strength. (B) Membrane curvature sensing assay was performed by mixing 20 μM IP3 with 40 nM BIN1-FL and (−) $PI(4,5)P_2$ GUVs in Hepes, 50 mM NaCl, pH 7.4 buffer.

CNM-Related SH3 Domain Truncation Abolishes BIN1 Autoinhibition. Centronuclear myopathy (CNM) is a congenital myopathy with abnormal cell nuclei displacement in skeletal muscles.[12,51,52] Mutations in the human BIN1 gene have been shown to cause CNM. Three single point mutations in the BAR domain region have been shown to interfere with the membrane tubulation capacity of BIN1 and to lead to disorganized T-tubules.[53−56] Two additional nonsense mutations were found to be located in the C-terminal SH3 domain.[54,56] Previous studies have suggested that CNM-related mutations in the SH3 domain disrupt the binding interface with proline-rich sequences and interfere with the ability to recruit dynamin 2. In fact, cellular experiments showed that the

dx.doi.org/10.1021/bi501082r | *Biochemistry* 2014, 53, 7297−7309

colocalization of BIN1 C-terminal mutants and dynamin 2 were decreased relative to BIN1-FL.[56] Because the SH3 domain binding interface for exon10 overlaps with that for the proline-rich domain,[11] we asked how the disease mutation at the SH3 domain C-terminus affects the autoinhibitory interaction with exon10.

First, to test if the SH3 domain bearing the CNM-associated mutation K436X can bind to exon10, we performed ITC measurements in which exon10 peptide (500 μM) was added to GST-SH3-K436X mutant (50 μM). Limited and constant amounts of heat were generated during the titration (Figure 8A). The ITC titration profile is similar to a control where exon10 peptides were titrated into pure buffer (Figure S2, Supporting Information). Compared to Figure 2B, we conclude that the truncation mutant K436X compromised the binding between SH3 domain and exon10 motif. We hypothesize that the deletion of the C-terminus disrupts the interface responsible for recruiting both exon10 motif and PRD peptide.

If the truncated SH3 domain is unable to associate with the exon10 motif, one would expect the autoinhibitory effect on the membrane curvature sensing and generation ability to vanish for this mutant. To test this hypothesis, tubulation assays were performed by incubating the CNM mutant K436X with liposomes with or without $PI(4,5)P_2$. In contrast to WT BIN1-FL, where tubulation was inhibited on (−) $PI(4,5)P_2$ membranes, tubulation was observed in both cases, independent of $PI(4,5)P_2$ (Figure 8B). This observation further supports the autoinhibition model in BIN1, which requires not only the co-presence but also the integrity of each binding partner.

Dynamin 2 is a large GTPase with diverse roles in cellular functions. Mutations in dynamin 2 contribute to deficits at the sarcotubular network indicating that misregulation of dynamin 2 leads to the pathogenesis of neuromuscular diseases.[57,58] Membrane recruitment of dynamin 2 via BIN1 is critical for healthy muscle development.[56] The SH3 domain is the module responsible for recruiting dynamin 2 by the interaction with PRD domains. We asked how autoinhibition of BIN1 can modulate the recruitment of downstream signaling molecules and whether activation of membrane remodeling and downstream ligand recruitment act in synergy.

To answer this question, we synthesized a rhodamine-labeled PRD peptide and incubated it with GUVs in the presence or absence of BIN1 variants. The PRD peptide itself does not bind to (+) $PI(4,5)P_2$ membranes in 50 mM NaCl (Figure 8C). Contrarily, on GUVs preincubated with 2 μM BIN1-FL (labeled with Alexa488 dye), significant enhancement of rhodamine fluorescence was observed (Figure 8C). Of note, images of vesicles were obtained at an excitation wavelength of 543 nm. To exclude bleed-through from Alexa488 into the rhodamine channel, imaging parameters (illumination intensity and detector settings) were carefully selected. In contrast to BIN1-FL, the disease mutant K436X is incapable of recruiting PRD peptides to the membranes (Figure 8C), consistent with the decreased dynamin 2 localization on BIN1-positive tubules in cells.[56] This supports the hypothesis that the PRD binding interface is disrupted in the truncation mutant. As a negative control, the coincubation with BIN1 N-BAR* domain failed to bind PRD peptides as well (Figure 8C), confirming that the recruitment of the PRD domain requires the presence and integrity of the SH3 domain.

To further understand the influence of phosphoinositides on dynamin 2 membrane recruitment, we repeated the PRD recruitment assay on (−) $PI(4,5)P_2$ membranes. We argue that

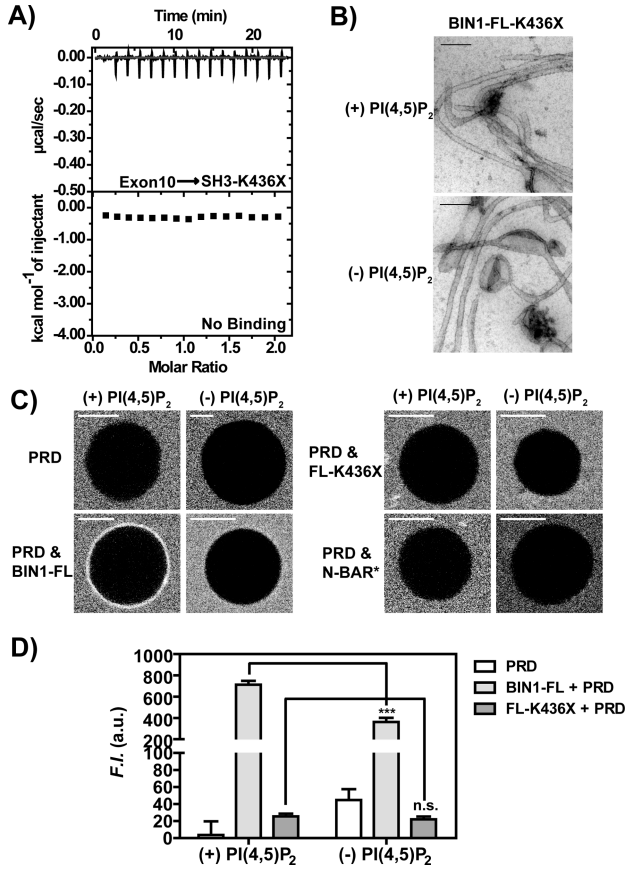

Figure 8. Autoinhibition is absent in the disease mutant K436X. Membrane recruitment of PRD peptide is enhanced by $PI(4,5)P_2$. (A) ITC measurement of titrating 500 μM exon10 peptide to 50 μM GST-SH3-K436X mutant indicates no detectable binding. Buffer: 20 mM Hepes, 150 mM NaCl, pH 7.4. (B) Electron micrographs of BIN1-FL-K436X mutants with LUVs (±) $PI(4,5)P_2$. K436X mutant is able to induce membrane tubules from liposomes lacking $PI(4,5)P_2$, implying that curvature generation capacity of K436X mutant is not regulated by $PI(4,5)P_2$. Scale bar: 200 nm. (C) Confocal fluorescence images of 2 μM rhodamine labeled PRD peptide only, or 2 μM PRD peptides mixed with 2 μM Alex488 labeled BIN1-FL, BIN1-FL-K436X, or N-BAR* on vesicles (±) $PI(4,5)P_2$. All images show the rhodamine channel under the excitation only by the 543 nm laser. BIN1-FL, but neither K436X mutant nor N-BAR* domain, is able to recruit dynamin 2 derived PRD peptide to the membrane. Scale bar: 5 μm. (D) Quantifications of the PRD fluorescence intensities (F.I.) in the absence/presence of BIN1-FL or BIN1-FL-K436X on (±) $PI(4,5)P_2$ vesicles. Comparison of the PRD fluorescence intensities in the presence of 2 μM BIN1-FL or BIN1-FL-K436X on vesicle (±) $PI(4,5)P_2$ was tested by Student's t-test. (+) $PI(4,5)P_2$ membranes show significantly enhanced membrane density of PRD peptides. n.s.: $p > 0.05$; ***: $p < 0.005$.

the presence of $PI(4,5)P_2$ in the membrane will compete with the SH3 domain to bind to the exon10 motif and increase the availability of the SH3 domain for PRD recruitment. Similarly, the PRD peptide does not bind to (−) $PI(4,5)P_2$ membranes on its own. Indeed, the signal of PRD peptides recruited by BIN1-FL on (−) $PI(4,5)P_2$ membranes is weaker than on (+) $PI(4,5)P_2$ membranes (Figure 8C). However, no PRD peptide is recruited to (−) $PI(4,5)P_2$ membranes via either the BIN1-FL-K436X mutant or the N-BAR* domain, as expected. We quantified PRD fluorescence at the membrane for each experimental condition. The decrease in the PRD membrane recruitment on (−) $PI(4,5)P_2$ membranes via BIN1 is

dx.doi.org/10.1021/bi501082r | Biochemistry 2014, 53, 7297−7309

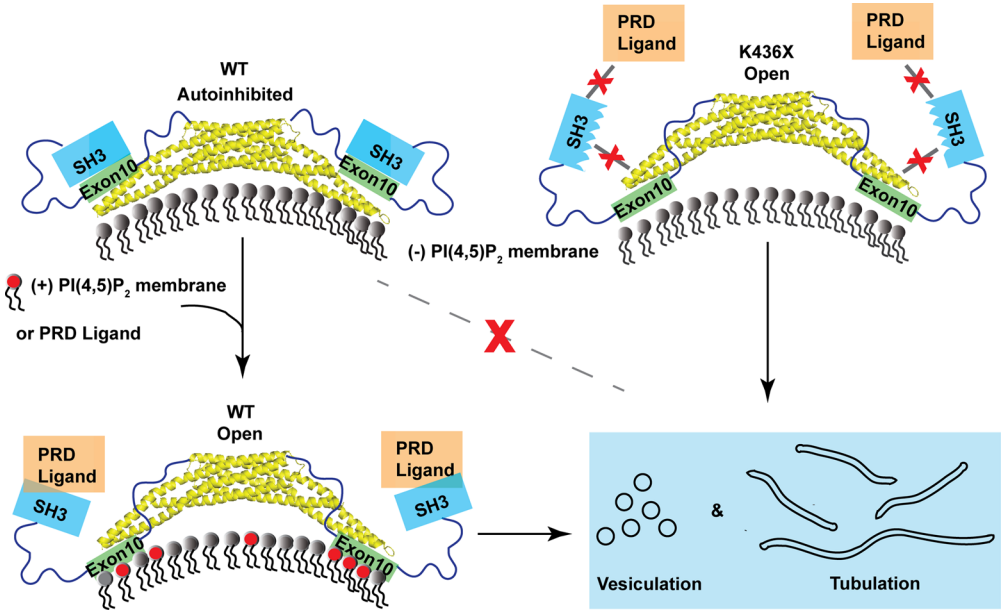

Figure 9. Proposed schematic illustration of how membrane composition and protein−ligand interaction cooperatively regulate membrane remodeling function of BIN1. BIN1-FL protein rests in a closed conformation through the interaction between SH3 and exon10 motifs. Exon10 is prevented from the interaction with membrane. Upon association with the membrane lacking $PI(4,5)P_2$, BIN1-FL protein is still blocked in the inactive state unable to sense or induce membrane deformation. Binding with $PI(4,5)P_2$ or the PRD containing proteins, such as dynamin 2 can induce an conformational change in BIN1 and activate MC-S&G. However, the CNM-related nonsense mutation disturbs the autoinhibitory interaction leading to an unregulated membrane modulation.

statistically significant (Figure 8D). Little PRD peptide is recruited by the K436X mutant to the membrane regardless of the lipid composition, further confirming that the functional SH3 domain is the key factor for recruiting downstream ligands. The weaker PRD membrane recruitment on (−) $PI(4,5)P_2$ membranes not only supports the autoinhibition model but also implies a synergistic regulation of BIN1 function through exon10-$PI(4,5)P_2$, and SH3 domain-ligand binding.

Phosphoinositides Slow BIN1 Diffusion on the Membrane. Protein oligomerization on membranes is an important mechanism contributing to MC-S&G by peripheral proteins.[44] It has been shown that BAR domain proteins form lattice-like coats on tubular membranes.[59] Protein oligomerization can amplify MC-S&G.[60] To ask whether the activation of BIN1 MC-S&G on (+) $PI(4,5)P_2$ membranes might be caused by effective protein assembly, we characterized the lateral diffusion of BIN1-FL on (±) $PI(4,5)P_2$ membranes via the fluorescence recovery after photobleaching (FRAP) method. BIN1-FL showed fluorescence recovery in the bleached region on both membrane compositions (Figure S3A, Supporting Information). However, the averaged recovery half-time $t_{1/2}$ of BIN1 on (+) $PI(4,5)P_2$ membranes is 2.5-fold slower than that on (−) $PI(4,5)P_2$ membranes. The averaged mobile fractions on (±) $PI(4,5)P_2$ membranes are not significantly different (Figure S3B−D). Recently, Lappalainen et al. reported that the F-BAR protein syp1 can induce $PI(4,5)P_2$ clusters, which act as hot spots for protein oligomeric assembly.[61] Consequently, the lateral diffusion of proteins on membranes is inhibited. It is likely that the slower BIN1-FL diffusion on membranes with $PI(4,5)P_2$ is caused by protein oligomerization. This assumption is consistent with the observation that a BAR domain mutant inefficient in oligomerization diffuses faster on the membrane.[61] The formation of oligomerized BIN1 networks on (+) $PI(4,5)P_2$ membranes might lead to enhanced MC-S&G.

DISCUSSION

One of the major findings of the present contribution is that the exon10 motif and C-terminal SH3 domain serve dual roles in regulating the function of BIN1. The exon10 motif causes autoinhibition via association with the SH3 domain and allows for membrane modulation by targeting $PI(4,5)P_2$. Similarly, the SH3 domain has two functions: autoinhibition and ligand recruitment. Autoinhibition is a regulatory mechanism found in other BAR domain proteins as well. It has been reported that various inputs work synergistically to regulate membrane localization and functional activation.[20,24] One example is the F-BAR domain protein syndapin1, which can form a molecular clamp between SH3 and BAR domain that leads to a compact, autoinhibited conformation unable to generate membrane curvature.[20,59] The activation of syndapin requires the binding of dynamin to the SH3 domain to induce an open conformation.[20,46] Such coupling between membrane curvature generation and dynamin recruitment was also found for endophilin/amphiphysin.[16] In fact, a great number of peripheral proteins contain domains, such as the SH3 domain, specialized for the recruitment of downstream ligands. Autoinhibition mediated by SH3 domains is also found in the cytoskeletal proteins N-WASP and IRSp53.[24,62,63] Intramolecular autoinhibition and simultaneous activation by specific membrane localization and ligand recruitment may be a general mechanism for proteins to control their function.

The autoinhibition model that we propose for BIN1 is shown schematically in Figure 9. BIN1 is in an inhibited state via the interaction between $PI(4,5)P_2$ sensing motif exon10 and SH3 domain, consistent with an earlier study showing that the exon10 peptide binds to the SH3 domain in a region overlapping with the binding interface of the proline-rich domain.[11] In the autoinhibited state, exon10 is masked from interacting with the membrane, and ligand recruitment through

dx.doi.org/10.1021/bi501082r | Biochemistry 2014, 53, 7297−7309

the SH3 domain is impaired. We showed that in the autoinhibited state, BIN1 still binds to, but cannot reshape the membrane. Upon membrane association, the local membrane composition becomes critical in determining if BIN1 is active or not. Particularly, $PI(4,5)P_2$ in the membrane plays an important role in releasing autoinhibition. On membranes where $PI(4,5)P_2$ is absent, BIN1 remains in a resting state, unable to sense and induce curvature (Figure 3 and 5). However, the presence of $PI(4,5)P_2$ in the membrane attracts exon10 away from the autoinhibitory interaction. This may explain the observation that T-tubules are enriched in $PI(4,5)P_2$ and that production of BIN1 and $PI(4,5)P_2$ during the differentiation of C2C12 cells is upregulated.[10] In addition to functional regulation by phosphoinositides, the binding of SH3 domain ligands to BIN1 results in activation of membrane remodeling (Figure 6). The synergy of the SH3 domain binding to other proteins along with membrane localization through $PI(4,5)P_2$ might be important for T-tubule biogenesis. Such cooperativity has also been reported for other BAR domain proteins with regard to their binding to dynamin and AP-2/clathrin in endocytosis.[64]

Moreover, we provided new insights into how CNM-related disease mutations in SH3 domain contribute to pathogenesis mechanisms (Figure 9). *In vivo* cellular experiments have suggested that the nonsense mutation in the SH3 domain compromised the recruitment of dynamin 2.[56] Our results not only support this claim but also show that the disease-related truncation of the SH3 domain interferes with autoinhibition through compromised binding to exon10 (Figure 8A). Consequently, the curvature sensing and generation ability of the K436X mutant is no longer regulated by $PI(4,5)P_2$ (Figure 8B). It can be hypothesized that active BIN1 adopts an open conformation favorable for membrane interaction. This assumption is supported by the finding that C-terminal disease mutants bind myotubularin (MTM1) more efficiently due to an increased accessibility of the MTM1 binding site in the open conformation.[65] Such conformational change is induced by the loss of the exon10−SH3 interaction. In summary, membrane remodeling by BIN1 is a synergistic process that involves correct membrane localization and ligand binding. It requires cooperative spatial and temporal assembly of proteins to precisely regulate the membrane deformation.

■ ASSOCIATED CONTENT

Supporting Information

CD spectrum of exon10 peptides in solution and on membranes (Figure S1), ITC control experiment by titrating exon10 peptides into buffer (Figure S2), lateral diffusion of BIN1-FL on (±) PI(4,5)P2 membranes studied by FRAP (Figure S3), and related experimental procedures. This material is available free of charge via the Internet at http://pubs.acs.org.

■ AUTHOR INFORMATION

Corresponding Author

*E-mail: baumgart@sas.upenn.edu.

Funding

This work was supported by National Institutes of Health (NIH) Grant R01 GM097552.

Notes

The authors declare no competing financial interest.

■ ACKNOWLEDGMENTS

We thank Dr. Tatyana Svitkina (University of Pennsylvania) for providing access to the transmission electron microscope (TEM) facility, Dr. Pietro De Camilli (Yale University) for providing the constructs of human wild type BIN1, and Dr. Christopher J. Lanci (Penn Biological Chemistry Resource Center) for help with peptide synthesis. We also thank Zheng Shi and Zhiming Chen for helpful discussions and proofreading of the manuscript.

■ ABBREVIATIONS

BAR, Bin/Amphiphysin/Rvs; T-tubules, transverse tubules; MC-S&G, membrane curvature sensing and generation; CNM, centronuclear myopathy; SH3, Src homology 3; PRD, proline-rich domain; ITC, isothermal titration calorimetry; SEM, standard error of the mean; GUV, giant unilamellar vesicle; TEM, transmission electron microscopy; LUV, large unilamellar vesicle; DOPC, 1,2-dioleoyl-*sn*-glycero-3-phosphocholine; DOPS, 1,2-dioleoyl-*sn*-glycero-3-phospho-L-serine; DOPE, 1,2-dioleoyl-*sn*-glycero-3-phosphoethanolamine; PI(4,5)P2, L-α-phosphatidylinositol-4,5-bisphosphate; TR-DHPE, TexasRed-1,2-dihexadecanoyl-*sn*-glycero-3-phos-phoethanolamine triethylammonium salt; IP3, D-myo-inositol-1,4,5-triphosphate; MTM1, myotubularin; DSPE-Bio-PEG2000, distearoylphosphatidylethanolamine-*N*-(biotinyl(polyethylene glycol)2000)

■ REFERENCES

(1) Qualmann, B., Koch, D., and Kessels, M. M. (2011) Let's go bananas: revisiting the endocytic BAR code. *EMBO J. 30*, 3501−3515.

(2) Mim, C., and Unger, V. M. (2012) Membrane curvature and its generation by BAR proteins. *Trends Biochem. Sci. 37*, 526−533.

(3) Al-Qusairi, L., and Laporte, J. (2011) T-tubule biogenesis and triad formation in skeletal muscle and implication in human diseases. *Skeletal Muscle 1*, 26−26.

(4) Butler, M. H., David, C., Ochoa, G. C., Freyberg, Z., Daniell, L., Grabs, D., Cremona, O., and DeCamilli, P. (1997) Amphiphysin II (SH3P9; BIN1), a member of the amphiphysin/Rvs family, is concentrated in the cortical cytomatrix of axon initial segments and nodes of Ranvier in brain and around T tubules in skeletal muscle. *J. Cell Biol. 137*, 1355−1367.

(5) Prokic, I., Cowling, B. S., and Laporte, J. (2014) Amphiphysin 2 (BIN1) in physiology and diseases. *J. Mol. Med. (Berlin) 92*, 453−463.

(6) Nance, J. R., Dowling, J. J., Gibbs, E. M., and Boennemann, C. G. (2012) Congenital Myopathies: An Update. *Curr. Neurol. Neurosci. Rep. 12*, 165−174.

(7) Casal, E., Federici, L., Zhang, W., Fernandez-Recio, J., Priego, E.-M., Miguel, R. N., DuHadaway, J. B., Prendergast, G. C., Luisi, B. F., and Laue, E. D. (2006) The crystal structure of the BAR domain from human Bin1/Amphiphysin II and its implications for molecular recognition. *Biochemistry 45*, 12917−12928.

(8) Ellis, J. D., Barrios-Rodiles, M., Colak, R., Irimia, M., Kim, T., Calarco, J. A., Wang, X., Pan, Q., O'Hanlon, D., Kim, P. M., Wrana, J. L., and Blencowe, B. J. (2012) Tissue-specific alternative splicing remodels protein-protein interaction networks. *Mol. Cell 46*, 884−892.

(9) Fugier, C., Klein, A. F., Hammer, C., Vassilopoulos, S., Ivarsson, Y., Toussaint, A., Tosch, V., Vignaud, A., Ferry, A., Messaddeq, N., Kokunai, Y., Tsuburaya, R., de la Grange, P., Dembele, D., Francois, V., Precigout, G., Boulade-Ladame, C., Hummel, M.-C., Lopez de Munain, A., Sergeant, N., Laquerriere, A., Thibault, C., Deryckere, F., Auboeuf, D., Garcia, L., Zimmermann, P., Udd, B., Schoser, B., Takahashi, M. P., Nishino, I., Bassez, G., Laporte, J., Furling, D., and Charlet-Berguerand, N. (2011) Misregulated alternative splicing of BIN1 is associated with T tubule alterations and muscle weakness in myotonic dystrophy. *Nat. Med. 17*, 720−725.

(10) Lee, E. Y., Marcucci, M., Daniell, L., Pypaert, M., Weisz, O. A., Ochoa, G. C., Farsad, K., Wenk, M. R., and De Camilli, P. (2002)

Amphiphysin 2 (Bin1) and T-tubule biogenesis in muscle. *Science 297*, 1193−1196.
(11) Kojima, C., Hashimoto, A., Yabuta, I., Hirose, M., Hashimoto, S., Kanaho, Y., Sumimoto, H., Ikegami, T., and Sabe, H. (2004) Regulation of Bin1 SH3 domain binding by phosphoinositides. *EMBO J. 23*, 4413−4422.
(12) Romero, N. B., and Bitoun, M. (2011) Centronuclear Myopathies. *Semin. Pediatr. Neurol. 18*, 250−256.
(13) Tjondrokoesoemo, A., Park, K. H., Ferrante, C., Komazaki, S., Lesniak, S., Brotto, M., Ko, J.-K., Zhou, J., Weisleder, N., and Ma, J. (2011) Disrupted Membrane Structure and Intracellular Ca(2+) Signaling in Adult Skeletal Muscle with Acute Knockdown of Bin1. *PLoS One 6*, e25740.
(14) Owen, D. J., Wigge, P., Vallis, Y., Moore, J. D. A., Evans, P. R., and McMahon, H. T. (1998) Crystal structure of the amphiphysin-2 SH3 domain and its role in the prevention of dynamin ring formation. *EMBO J. 17*, 5273−5285.
(15) Sundborger, A., Soderblom, C., Vorontsova, O., Evergren, E., Hinshaw, J. E., and Shupliakov, O. (2011) An endophilin-dynamin complex promotes budding of clathrin-coated vesicles during synaptic vesicle recycling. *J. Cell Sci. 124*, 133−143.
(16) Meinecke, M., Boucrot, E., Camdere, G., Hon, W.-C., Mittal, R., and McMahon, H. T. (2013) Cooperative Recruitment of Dynamin and BIN/Amphiphysin/Rvs (BAR) Domain-containing Proteins Leads to GTP-dependent Membrane Scission. *J. Biol. Chem. 288*, 6651−6661.
(17) Feng, S. B., Chen, J. K., Yu, H. T., Simon, J. A., and Schreiber, S. L. (1994) Two Binding Orientations for Peptides to the Src SH3 Domain - Development of a General-Model for SH3-Ligand Interactions. *Science 266*, 1241−1247.
(18) Fu, C. J., Wu, G., Lv, F. L., and Tian, F. F. (2012) Structure-based characterization of the binding of peptide to the human endophilin-1 Src homology 3 domain using position-dependent noncovalent potential analysis. *J. Mol. Model. 18*, 2153−2161.
(19) Anggono, V., and Robinson, P. J. (2007) Syndapin I and endophilin I bind overlapping proline-rich regions of dynamin I: role in synaptic vesicle endocytosis. *J. Neurochem. 102*, 931−943.
(20) Rao, Y., Ma, Q., Vahedi-Faridi, A., Sundborger, A., Pechstein, A., Puchkov, D., Luo, L., Shupliakov, O., Saenger, W., and Haucke, V. (2010) Molecular basis for SH3 domain regulation of F-BAR-mediated membrane deformation. *Proc. Natl. Acad. Sci. U.S.A. 107*, 8213−8218.
(21) Chen, Z., Chang, K., Capraro, B. R., Zhu, C., Hsu, C.-J., and Baumgart, T. (2014) Intradimer/Intermolecular interactions suggest autoinhibition mechanism in endophilin A1. *J. Am. Chem. Soc. 136*, 4557−4564.
(22) Vazquez, F. X., Unger, V. M., and Voth, G. A. (2013) Autoinhibition of Endophilin in Solution via Interdomain Interactions. *Biophys. J. 104*, 396−403.
(23) Walde, P., Cosentino, K., Engel, H., and Stano, P. (2010) Giant Vesicles: Preparations and Applications. *ChemBioChem 11*, 848−865.
(24) Kast, D. J., Yang, C., Disanza, A., Boczkowska, M., Madasu, Y., Scita, G., Svitkina, T., and Dominguez, R. (2014) Mechanism of IRSp53 inhibition and combinatorial activation by Cdc42 and downstream effectors. *Nat. Struct. Mol. Biol. 21*, 413−422.
(25) Hertzog, M., Milanesi, F., Hazelwood, L., Disanza, A., Liu, H., Perlade, E., Malabarba, M. G., Pasqualato, S., Maiolica, A., Confalonieri, S., Le Clainche, C., Offenhauser, N., Block, J., Rottner, K., Di Fiore, P. P., Carlier, M.-F., Volkmann, N., Hanein, D., and Scita, G. (2010) Molecular Basis for the Dual Function of Eps8 on Actin Dynamics: Bundling and Capping. *PLoS Biol. 8*, e1000387.
(26) Grabs, D., Slepnev, V. I., Zhou, S. Y., David, C., Lynch, M., Cantley, L. C., and DeCamilli, P. (1997) The SH3 domain of amphiphysin binds the proline-rich domain of dynamin at a single site that defines a new SH3 binding consensus sequence. *J. Biol. Chem. 272*, 13419−13425.
(27) Ladokhin, A. S., Fernandez-Vidal, M., and White, S. H. (2010) CD Spectroscopy of Peptides and Proteins Bound to Large Unilamellar Vesicles. *J. Membr. Biol. 236*, 247−253.
(28) Jung, A. G., Labarerra, C., Jansen, A. M., Qvortrup, K., Wild, K., and Kjaerulff, O. (2010) A Mutational Analysis of the Endophilin-A N-BAR Domain Performed in Living Flies. *PLoS One 5*, e9492.
(29) Farsad, K., Ringstad, N., Takei, K., Floyd, S. R., Rose, K., and De Camilli, P. (2001) Generation of high curvature membranes mediated by direct endophilin bilayer interactions. *J. Cell Biol. 155*, 193−200.
(30) Boucrot, E., Pick, A., Camdere, G., Liska, N., Evergren, E., McMahon, H. T., and Kozlov, M. M. (2012) Membrane Fission Is Promoted by Insertion of Amphipathic Helices and Is Restricted by Crescent BAR Domains. *Cell 149*, 124−136.
(31) Bhatia, V. K., Hatzakis, N. S., and Stamou, D. (2010) A unifying mechanism accounts for sensing of membrane curvature by BAR domains, amphipathic helices and membrane-anchored proteins. *Semin. Cell Dev. Biol. 21*, 381−390.
(32) Fernandes, F., Loura, L. M. S., Chichon, F. J., Carrascosa, J. L., Fedorov, A., and Prieto, M. (2008) Role of helix 0 of the N-BAR domain in membrane curvature generation. *Biophys. J. 94*, 3065−3073.
(33) Morton, L. A., Yang, H., Saludes, J. P., Fiorini, Z., Beninson, L., Chapman, E. R., Fleshner, M., Xue, D., and Yin, H. (2013) MARCKS-ED Peptide as a Curvature and Lipid Sensor. *ACS Chem. Biol. 8*, 218−225.
(34) Porumb, T., Crivici, A., Blackshear, P. J., and Ikura, M. (1997) Calcium binding and conformational properties of calmodulin complexed with peptides derived from myristoylated alanine-rich C kinase substrate (MARCKS) and MARCKS-related protein (MRP). *Eur. Biophys. J. 25*, 239−247.
(35) Zhu, C., Das, S. L., and Baumgart, T. (2012) Nonlinear Sorting, Curvature Generation, and Crowding of Endophilin N-BAR on Tubular Membranes. *Biophys. J. 102*, 1837−1845.
(36) Sorre, B., Callan-Jones, A., Manzi, J., Goud, B., Prost, J., Bassereau, P., and Roux, A. (2012) Nature of curvature coupling of amphiphysin with membranes depends on its bound density. *Proc. Natl. Acad. Sci. U.S.A. 109*, 173−178.
(37) Wu, T., Shi, Z., and Baumgart, T. (2014) Mutations in BIN1 Associated with Centronuclear Myopathy Disrupt Membrane Remodeling by Affecting Protein Density and Oligomerization. *PLoS One 9*, e93060.
(38) Ellenbroek, W. G., Wang, Y.-H., Christian, D. A., Discher, D. E., Janmey, P. A., and Liu, A. J. (2011) Divalent Cation-Dependent Formation of Electrostatic PIP2 Clusters in Lipid Monolayers. *Biophys. J. 101*, 2178−2184.
(39) McLaughlin, S., Wang, J., Gambhir, A., and Murray, D. (2002) PIP2 and Proteins: Interactions, Organization and Information Flow. *Annu. Rev. Biophys. Biomol. Struct. 31*, 151−175.
(40) Toner, M., Vaio, G., McLaughlin, A., and McLaughlin, S. (1988) Adsorption of Cations to Phosphatidylinositol 4,5-Bisphosphate. *Biochemistry 27*, 7435−7443.
(41) Wang, J. Y., Arbuzova, A., Hangyas-Mihalyne, G., and McLaughlin, S. (2001) The effector domain of myristoylated alanine-rich C kinase substrate binds strongly to phosphatidylinositol 4,5-bisphosphate. *J. Biol. Chem. 276*, 5012−5019.
(42) Sorre, B., Callan-Jones, A., Manneville, J.-B., Nassoy, P., Joanny, J.-F., Prost, J., Goud, B., and Bassereau, P. (2009) Curvature-driven lipid sorting needs proximity to a demixing point and is aided by proteins. *Proc. Natl. Acad. Sci. U.S.A. 106*, 5622−5626.
(43) Capraro, B. R., Yoon, Y., Cho, W., and Baumgart, T. (2010) Curvature Sensing by the Epsin N-Terminal Homology Domain Measured on Cylindrical Lipid Membrane Tethers. *J. Am. Chem. Soc. 132*, 1200−1201.
(44) Baumgart, T., Capraro, B. R., Zhu, C., and Das, S. L. (2011) Thermodynamics and Mechanics of Membrane Curvature Generation and Sensing by Proteins and Lipids. *Annu. Rev. Phys. Chem. 62*, 483−506.
(45) Yoon, Y., Zhang, X., and Cho, W. (2012) Phosphatidylinositol 4,5-Bisphosphate (PtdIns(4,5)P-2) Specifically Induces Membrane Penetration and Deformation by Bin/Amphiphysin/Rvs (BAR) Domains. *J. Biol. Chem. 287*, 34078−34090.

(46) Goh, S. L., Wang, Q., Byrnes, L. J., and Sondermann, H. (2012) Versatile Membrane Deformation Potential of Activated Pacsin. *PLoS One 7*, e51628.
(47) Spector, A. A., and Yorek, M. A. (1985) Membrane lipid composition and cellular function. *J. Lipid Res. 26*, 1015−1035.
(48) Kishore, A. I., and Prestegard, J. H. (2003) Molecular orientation and conformation of phosphatidylinositides in membrane mimetics using variable angle sample spinning (VASS) NMR. *Biophys. J. 85*, 3848−3857.
(49) Ambroso, M. R., Hegde, B. G., and Langen, R. (2014) Endophilin A1 induces different membrane shapes using a conformational switch that is regulated by phosphorylation. *Proc. Natl. Acad. Sci. U.S.A. 111*, 6982−6987.
(50) Harder, D. R. (1983) Heterogeneity of Membrane-Properties in Vascular Muscle-Cells from Various Vascular Beds. *Fed. Proc. 42*, 253−256.
(51) Jungbluth, H., Wallgren-Pettersson, C., and Laporte, J. (2008) Centronuclear (myotubular) myopathy. *Orphanet J. Rare Dis. 3*, 26.
(52) Romero, N. B. (2010) Centronuclear myopathies: A widening concept. *Neuromuscul. Disord. 20*, 223−228.
(53) Toussaint, A., Cowling, B. S., Hnia, K., Mohr, M., Oldfors, A., Schwab, Y., Yis, U., Maisonobe, T., Stojkovic, T., Wallgren-Pettersson, C., Laugel, V., Echaniz-Laguna, A., Mandel, J.-L., Nishino, I., and Laporte, J. (2011) Defects in amphiphysin 2 (BIN1) and triads in several forms of centronuclear myopathies. *Acta Neuropathol. 121*, 253−266.
(54) Boehm, J., Yis, U., Ortac, R., Cakmakci, H., Kurul, S. H., Dirik, E., and Laporte, J. (2010) Case report of intrafamilial variability in autosomal recessive centronuclear myopathy associated to a novel BIN1 stop mutation. *Orphanet J. Rare Dis. 5*, 35.
(55) Claeys, K. G., Maisonobe, T., Boehm, J., Laporte, J., Hezode, M., Romero, N. B., Brochier, G., Bitoun, M., Carlier, R. Y., and Stojkovic, T. (2010) Phenotype of a Patient with Recessive Centronuclear Myopathy and a Novel Bin1 mutation. *Neurology 74*, 519−521.
(56) Nicot, A.-S., Toussaint, A., Tosch, V., Kretz, C., Wallgren-Pettersson, C., Iwarsson, E., Kingston, H., Garnier, J.-M., Biancalana, V., Oldfors, A., Mandel, J.-L., and Laporte, J. (2007) Mutations in amphiphysin 2 (BIN1) disrupt interaction with dynamin 2 and cause autosomal recessive centronuclear myopathy. *Nat. Genet. 39*, 1134−1139.
(57) Durieux, A.-C., Prudhon, B., Guicheney, P., and Bitoun, M. (2010) Dynamin 2 and human diseases. *J. Mol. Med. 88*, 339−350.
(58) Demonbreun, A. R., and McNally, E. M. (2014) Dynamin 2 the rescue for centronuclear myopathy. *J. Clin. Invest. 124*, 976−978.
(59) Frost, A., Perera, R., Roux, A., Spasov, K., Destaing, O., Egelman, E. H., De Camilli, P., and Unger, V. M. (2008) Structural basis of membrane invagination by F-BAR domains. *Cell 132*, 807−817.
(60) Roux, A., Koster, G., Lenz, M., Sorre, B., Manneville, J.-B., Nassoy, P., and Bassereau, P. (2010) Membrane curvature controls dynamin polymerization. *Proc. Natl. Acad. Sci. U.S.A. 107*, 4141−4146.
(61) Zhao, H., Michelot, A., Koskela, E. V., Tkach, V., Stamou, D., Drubin, D. G., and Lappalainen, P. (2013) Membrane-Sculpting BAR Domains Generate Stable Lipid Microdomains. *Cell Rep. 4*, 1213−1223.
(62) Kim, A. S., Kakalis, L. T., Abdul-Manan, M., Liu, G. A., and Rosen, M. K. (2000) Autoinhibition and activation mechanisms of the Wiskott-Aldrich syndrome protein. *Nature 404*, 151−158.
(63) Abdul-Manan, N., Aghazadeh, B., Liu, G. A., Majumdar, A., Ouerfelli, O., Siminovitch, K. A., and Rosen, M. K. (1999) Structure of Cdc42 in complex with the GTPase-binding domain of the 'Wiskott-Aldrich syndrome' protein. *Nature 399*, 379−383.
(64) Farsad, K., Slepnev, V., Ochoa, G. C., Daniell, L., Haucke, V., and De Camilli, P. (2004) A putative role for intramolecular regulatory mechanisms in the adaptor function of amphiphysin in endocytosis. *Neuropharmacology 46*, 297−297.
(65) Royer, B., Hnia, K., Gavriilidis, C., Tronchere, H., Tosch, V., and Laporte, J. (2013) The myotubularin-amphiphysin 2 complex in membrane tubulation and centronuclear myopathies. *EMBO Rep. 14*, 907−915.